CHEMISTRY
A EUROPEAN JOURNAL

DOI: 10.1002/chem.200701598

The Isomers of Gadolinium Scandium Nitride Clusterfullerenes $Gd_xSc_{3-x}N@C_{80}$ ($x=1$, 2) and Their Influence on Cluster Structure

Shangfeng Yang,*[a] Alexey Popov,[a, b] Martin Kalbac,[a, c] and Lothar Dunsch*[a]

Abstract: The isomers of gadolinium scandium mixed-metal nitride clusterfullerenes $Gd_xSc_{3-x}N@C_{80}$ [$x=2$ (**1**, **4**); $x=1$ (**2**, **5**)] have been synthesized by the "reactive gas atmosphere" method and isolated facilely by recycling HPLC. The yield of $Gd_xSc_{3-x}N@C_{80}$ (I, II) ($x=1$, 2) relative to the homogenous clusterfullerenes $Sc_3N@C_{80}$ [I (**3**), II (**6**)] was determined. According to the UV/Vis/NIR spectroscopic data, **1**, **2**, **4**, and **5** are all stable fullerenes with large optical gaps. Fullerene **1** has greater similarity to $Gd_3N@C_{80}$ (I) and **2** seems to resemble $Sc_3N@C_{80}$ (I). The quite similar overall absorption features of **4** and **5** suggest pronounced similarity in electronic structure. Vibrational spectroscopic studies led to the assignment of the cage symmetries of $Gd_xSc_{3-x}N@C_{80}$ (I, II), that is, I_h for **1**, **2** and D_{5h} for **4**, **5**. The cluster–cage interactions in $Gd_xSc_{3-x}N@C_{80}$ (I, II) were analyzed by means of the low-energy Raman lines. The splitting of the metal–nitrogen stretching vibrational mode in $Gd_xSc_{3-x}N@C_{80}$ (I, II) was studied in detail. Scalar-relativistic DFT calculations were performed to reveal the geometry parameters and the magnetic state of the $Gd_xSc_{3-x}N@C_{80}$ (I, II) molecules.

Keywords: cluster compounds · fullerenes · lanthanides · structure elucidation · vibrational spectroscopy

Introduction

As a new class of fullerenes with an encaged trimetallic nitride cluster, the trimetallic nitride endohedral fullerenes (clusterfullerenes) have attracted great interest due to their feasibility of varying the trapped metal atoms and of stabilizing a large variety of cage sizes and different isomeric structures.[1–5] In particular, the mixed-metal nitride clusterfullerenes, that is, nitride clusterfullerenes with two different metals in the encaged nitride, are recognized as minor members of the clusterfullerene family.[1] The few mixed-metal clusterfullerenes so far reported include $Er_xSc_{3-x}N@C_{80}$ ($x=0$–2),[1,2,6] $A_xSc_{3-x}N@C_{68}$ ($x=0$–2; A = Tm, Er, Gd, Ho, La),[7] $Lu_{3-x}A_xN@C_{80}$ ($x=0$–2; A = Gd, Ho),[8] $CeSc_2N@C_{80}$,[9] and $Sc_{3-x}Y_xN@C_{80}$ ($x=0$–3).[10] The modest progress achieved to date in the isolation of the mixed-metal clusterfullerenes is largely due to difficulties in their HPLC separation, as clusterfullerenes with different cluster composition but the same carbon cage isomer exhibit a very similar HPLC behavior.[1,6,9] Nevertheless, a noteworthy feature of the mixed-metal nitride clusterfullerenes is that their yields can exceed those of the homogeneous metal nitride clusterfullerenes.[1,2,7,8] Such an advantage makes the mixed-metal nitride clusterfullerenes a promising matrix to boost the yield of clusterfullerenes, which is quite low in the form of homogeneous metal nitride clusterfullerenes.

Fullerenes of larger cage sizes exist in isomeric forms.[11] For C_{80}-based homogeneous nitride clusterfullerenes, the coexistence of a second isomer which shows quite a different cage structure and electronic properties to the first isomer (C_{80}:I_h) has been already elucidated for $M_3N@C_{80}$ (M = Sc, Tm, Gd, Dy).[1,4a,5a–c] However, in the case of mixed-metal nitride clusterfullerenes, only the C_{80}:I_h cage has been isolated within $ErSc_2N@C_{80}$, $CeSc_2N@C_{80}$, $Er_2ScN@C_{80}$, and $Sc_{3-x}Y_xN@C_{80}$ ($x=0$–3), the structures of which were determined by X-ray crystallography or spectroscopy.[6,9,10] Therefore, an open question is whether cage isomers other than

[a] Dr. S. Yang, Dr. A. Popov, Dr. M. Kalbac, Prof. Dr. L. Dunsch
Group of Electrochemistry and Conducting Polymers
Leibniz-Institute for Solid State and Materials Research
Dresden, 01171 Dresden (Germany)
Fax: (+49) 351-4659-745
E-mail: s.yang@ifw-dresden.de
l.dunsch@ifw-dresden.de

[b] Dr. A. Popov
Department of Chemistry, Moscow State University
Leninskiye Gory, 119992 Moscow (Russia)

[c] Dr. M. Kalbac
J. Heyrovský Institute of Physical Chemistry
Academy of Sciences of the Czech Republic
Dolejškova 3, 18223 Prague 8 (Czech Republic)

Supporting information for this article is available on the WWW under http://www.chemeurj.org/ or from the author.

the I_h isomer could be isolated for the mixed-metal nitride clusterfullerenes. Furthermore, it is important to address whether the yield of other isomers of C_{80}-based mixed-metal nitride clusterfullerenes is higher than that of the homogenous metal nitride clusterfullerenes, as in the case of the I_h isomer.

Recently we reported the isolation and characterization of the first isomer of $Gd_xSc_{3-x}N@C_{80}$ (I_h) ($x=1$, 2), and found an enhanced yield of $GdSc_2N@C_{80}$ (I) in comparison to $Sc_3N@C_{80}$ (I), and a dramatically enhanced yield of $Gd_xSc_{3-x}N@C_{80}$ (I_h) compared to $Gd_3N@C_{80}$ (I).[12] More recently, studies on pyrrolidino derivatives of $Gd_xSc_{3-x}N@C_{80}$ (I) ($x=0$–3) by Wang et al. revealed that the regioselectivity of $Gd_{3-x}Sc_xN@C_{80}$ (I) ($x=0$–3) in exohedral cycloadditions depends remarkably on the size of the encaged cluster.[13]

Herein we report for the first time the synthesis and facile HPLC isolation of two isomers of Sc/Gd mixed-metal nitride clusterfullerenes $Gd_xSc_{3-x}N@C_{80}$ (I, II) ($x=1$, 2). The yield of $Gd_xSc_{3-x}N@C_{80}$ (I, II) ($x=1$, 2) relative to the homogenous metal nitride clusterfullerenes $Sc_3N@C_{80}$ (I, II) was calculated. The isolated $Gd_xSc_{3-x}N@C_{80}$ (I, II) ($x=1$, 2) were characterized by mass spectrometry and UV/Vis/NIR, FTIR, and Raman spectroscopy. The cage structures of $Gd_xSc_{3-x}N@C_{80}$ (I, II) ($x=1$, 2) were determined by means of their vibrational spectra. Based on scalar-relativistic DFT calculations the structures and magnetic properties of the encaged $Gd_xSc_{3-x}N$ mixed nitride clusters are discussed in detail. An interplay of cage symmetry and cluster structure is demonstrated for these mixed-metal nitride cluster fullerenes.

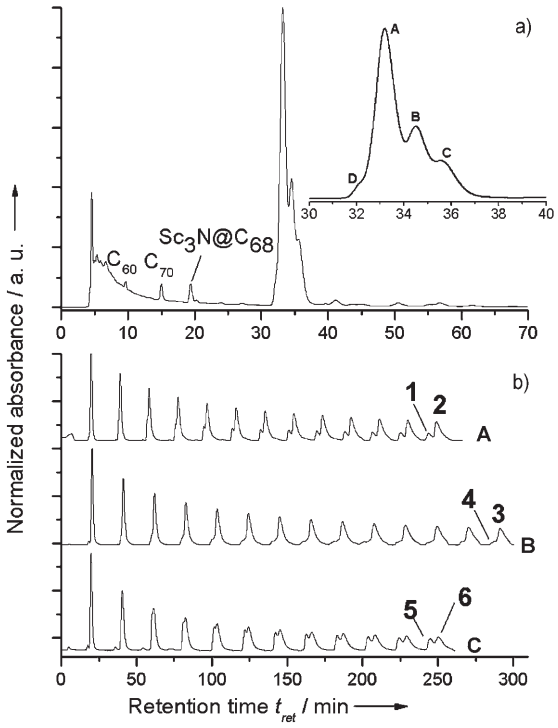

Figure 1. a) Chromatogram of a $Gd_xSc_{3-x}N@C_{2n}$ fullerene extract mixture synthesized by the "reactive gas atmosphere" method (linear combination of two 4.6×250 mm Buckyprep columns; flow rate 1.6 mL min^{-1}; injection volume 100 μL; toluene as eluent; 40 °C). The inset shows the enlarged chromatographic region of the dominant fractions A–D, which correspond to $Gd_xSc_{3-x}N@C_{2n}$ (I, II) ($x=0$–3, $2n=78$, 80). b) Chromatograms of fractions A–C isolated by recycling HPLC (10×250 mm Buckyprep-M column; flow rate 5.0 mL min^{-1}; injection volume 5 mL; toluene as eluent; 25 °C).

Results and Discussion

Synthesis and isolation of $Gd_xSc_{3-x}N@C_{80}$ (I, II; $x=1$, 2) clusterfullerenes: Figure 1a shows a typical chromatogram of a $Gd_xSc_{3-x}@C_{2n}$ fullerene extract mixture obtained under optimized conditions (molar ratio of Gd:Sc:C=1:1:15) by the "reactive gas atmosphere" method.[1,3–5,12] According to the mass spectrometric (MS) analysis, the abundance of the dominant products, which are two isomers of $Gd_xSc_{3-x}N@C_{80}$ (I & II, $x=0$–3; see fractions A–C in the inset of Figure 1a), reaches up to 97% of all the fullerenes. Significantly, the yields of $Gd_xSc_{3-x}N@C_{80}$ (I & II, $x=0$–3) is dramatically higher than that of $Gd_3N@C_{80}$, as revealed previously.[12]

Two isomers of $Gd_xSc_{3-x}N@C_{80}$ ($x=1$, 2) were isolated by a two-step HPLC with recycling HPLC in the second step. By using a linear combination of two Buckyprep columns in the first-stage HPLC, fractions A–D were isolated, each of which contains at least two different $Gd_xSc_{3-x}N@C_{2n}$ ($x=0$–3, $2n=78$, 80) products. Fractions A–C were then subjected to second-stage isolation by recycling HPLC on a Buckyprep-M column, as shown in Figure 1b. Thus, all three fractions were isolated on recycling 13, 14, and 12 times for fractions A, B, and C, respectively, as identified by laser-desorption time-of-flight (LD-TOF) MS analysis (Figure 2), which confirmed their high purity (≥99%) as well. The fairly good agreement of the measured isotope distributions of $Gd_xSc_{3-x}N@C_{80}$ (I, II; $x=1$, 2) with the theoretical calculations confirms the proposed chemical forms (see Figure 2b). Among them, isomer I of $Gd_xSc_{3-x}N@C_{80}$ (**1**, $x=2$; **2**, $x=1$) is obtained in fraction A, while isomer II of $Gd_xSc_{3-x}N@C_{80}$ (**4**, $x=2$; **5**, $x=1$) is co-eluted with $Sc_3N@C_{80}$ (I) (**3**) and $Sc_3N@C_{80}$ (II) (**6**) in fractions B and C, respectively. This indicates a distinct difference in retention time in the first-stage HPLC on the Buckyprep columns because of their different molecular and electronic structures.

Under the optimized synthesis condition (molar ratio of Gd:Sc:C=1:1:15), the sum of yields of **1** and **2** was 30–40 times higher than that of $Gd_3N@C_{80}$ (I).[12] In addition, based on the integrated areas of the corresponding chromatographic peaks (Figure 3), the relative yield of **1**:**2**:**3** was calculated to be about 0.56:2.2:1 in a previous study, that is the mixed metals have a boosting effect on the yield of $Gd_xSc_{3-x}N@C_{80}$ (I) compared to the homogeneous nitride clusterfullerenes.[12] In the same way the relative yield of **4**:**5**:**6** was calculated to be 0.36:0.8:1 (see Figure 3), that is, **4** and **5** [i.e., $Gd_xSc_{3-x}N@C_{80}$ (II)] have a lower yield than $Sc_3N@C_{80}$ (II) (**6**). These results suggest that the effect of the mixed-metal composition and cluster size on the forma-

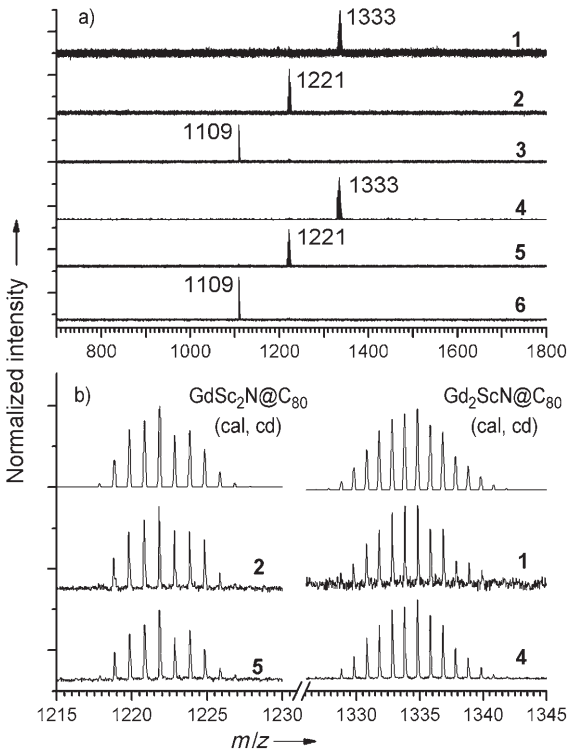

Figure 2. a) Positive-ion LD-TOF mass spectra of isolated $Gd_xSc_{3-x}N@C_{80}$ (I, II) (**1**–**6**). b) Measured and calculated isotope distributions of $Gd_xSc_{3-x}N@C_{80}$ (I, II).

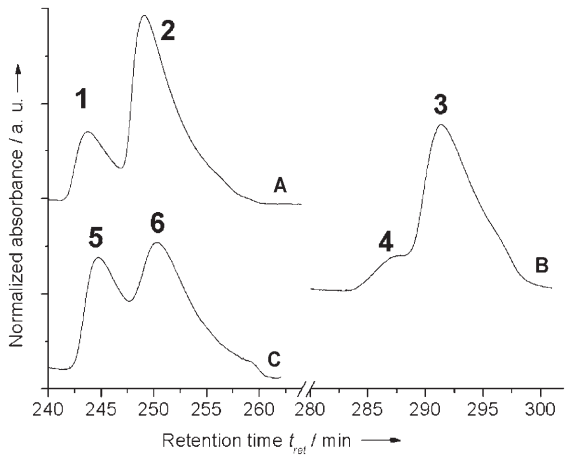

Figure 3. Chromatograms of fractions A–C in the final cycle by recycling HPLC (based on Figure 1b).

tion of Sc/Gd clusterfullerenes varies for different isomer structures.

Electronic absorption spectra of isolated $Gd_xSc_{3-x}N@C_{80}$ (I, II) ($x=1$, 2): UV/Vis/NIR spectra of the isolated $Gd_xSc_{3-x}N@C_{80}$ (I, II) ($x=0$–3, **1**–**6**) dissolved in toluene are shown in Figure 4, and their characteristic absorption data are summarized in Table 1. Detailed analysis of the electronic absorption features of **1** and **2** [$Gd_xSc_{3-x}N@C_{80}$ (I) ($x=1$, 2)] has been reported previously (see Figure 4a).[12] In brief, the overall absorption pattern of $Gd_3N@C_{80}$ (I) is largely preserved in **1**, while the spectrum of **2** is more reminiscent of that of $Sc_3N@C_{80}$ (I) (**3**). This shows how the electronic structure of $Gd_xSc_{3-x}N@C_{80}$ (I) varies with the composition of the $Gd_xSc_{3-x}N$ cluster.[12]

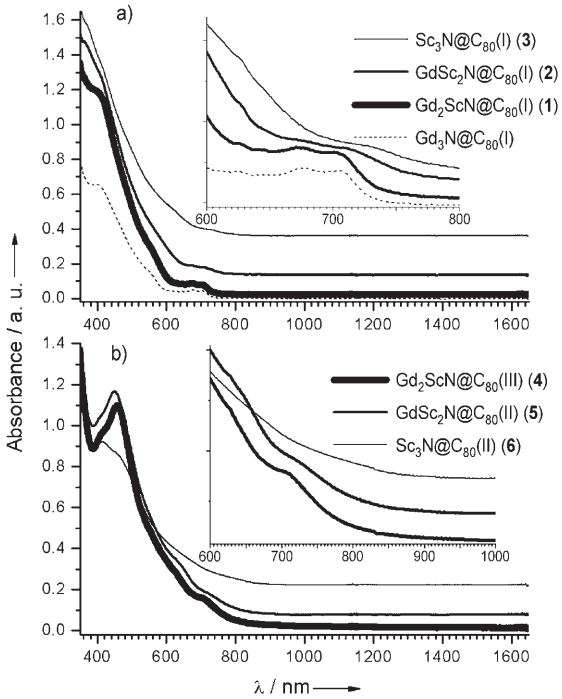

Figure 4. UV/Vis/NIR spectra of the two isomers of $Gd_xSc_{3-x}N@C_{80}$ (x=0–3) dissolved in toluene (I, a; II, b). The insets show enlarged spectral ranges.

The electronic absorption spectra of $Gd_xSc_{3-x}N@C_{80}$ (II) (**4** and **5**) are clearly different from those of isomer I, which falls in line with the differences in the absorption spectra of isomers I and II reported earlier for homogeneous clusters.[1,4a,5a–c] Likewise, significant variation in electronic structure of the cage with changing composition of the $Gd_xSc_{3-x}N$ cluster takes place in $Gd_xSc_{3-x}N@C_{80}$ (II) (Figure 4b). For instance, the absorption peak at 705 nm observed in the spectrum of **4** is red-shifted to about 724 nm in that of **5** and becomes indistinguishable from that of $Sc_3N@C_{80}$ (II) (**6**) (see inset of Figure 4b). In the higher energy range, the shoulder peak at 629 nm in the spectrum of **4** undergoes similar transformations in the spectra of **5** and **6**, while the strongest absorption peak in the visible range of **4** at 455 nm is slightly blue-shifted to 450 nm in **5**, whereas the shoulder peak at about 408 nm in **4** remains unchanged in **5**. In the spectrum of **6** these two absorption peaks are both red-shifted, with absorption maxima at 413 and 472 nm. The overall absorption spectrum of **4** is quite similar to that of **5**, and this suggests strong resemblance of their electronic structures.

Besides the similarity/difference in the characteristic electronic absorptions of **4**–**6**, their onsets of spectral absorption are quite close: 980, 960, and 950 nm for **4**, **5** and **6**, respec-

Table 1. Characteristics of $Gd_xSc_{3-x}N@C_{80}$ (I, II) clusterfullerenes.

x	No.	Product	m/z	UV/Vis/NIR absorption peaks [nm]	Onset [nm]	Band gap[a] [eV]	$\tilde{\nu}_{Sc-N}$[b] [cm^{-1}]	$\tilde{\nu}_{Gd-N}$[b] [cm^{-1}]	$\tilde{\nu}_{def}$[c] [cm^{-1}]	Cage symmetry[d]	Cluster structure
3		$Gd_3N@C_{80}$ (I)	1445	402, 554, 706, 676	780	1.59		657	165	7:I_h	pyramidal
2	**1**	$Gd_2ScN@C_{80}$ (I)	1333	402, 555, 703, 672	810	1.53	759	649, 656	165, 210	7:I_h	planar
1	**2**	$GdSc_2N@C_{80}$ (I)	1221	411, 712	820	1.51	694	647	167, 210	7:I_h	planar
0	**3**	$Sc_3N@C_{80}$(I)	1109	424, 735	820	1.51	599		210	7:I_h	planar
2	**4**	$Gd_2ScN@C_{80}$ (II)	1333	408, 455, 629, 705	980	1.26	743	647		6:D_{5h}	planar
1	**5**	$GdSc_2N@C_{80}$ (II)	1221	408, 450, 641, 724	960	1.29	687	634	164, 209	6:D_{5h}	planar
0	**6**	$Sc_3N@C_{80}$ (II)	1109	413, 472	950	1.30	595		209	6:D_{5h}	planar

[a] The band gap was estimated and converted from the onset (band gap [eV] $\approx$ 1240/onset [nm]). [b] Antisymmetric M–N stretching frequency. [c] Cluster deformation mode of $Gd_xSc_{3-x}N$. [d] The symbols of the C_{80} isomer are based on ref. [11]

tively, so that **4–6** have comparable optical band gaps of about 1.3 eV (see Table 1).

Vibrational spectra and assignment of the cage structures of $Gd_xSc_{3-x}N@C_{80}$ (I, II) (x = 1, 2): As we have shown in our recent studies, the high structural sensitivity of IR spectroscopy in combination with DFT calculations has been developed into a feasible method for structure elucidation of nitride clusterfullerenes.[1,3–5,12] The FTIR spectra of $Gd_xSc_{3-x}N@C_{80}$ (I) (x = 0–3), which are compared in Figure 5a, clearly indicate the identity of their cage vibrational modes (both tangential and radial).[12] This enables us to assign the same cage isomer of the reported $M_3N@C_{80}$ (I) (M = Gd, Sc), that is, C_{80}:7 with I_h symmetry,[1,3–5,12] to the carbon cages of **1** and **2** (see Figure 9 below). Likewise, based on the close resemblances observed for the FTIR spectra of **4–6** as shown in Figure 5b,[14] we conclude that the cage of **4** and **5** have the same structure as that of $Sc_3N@C_{80}$ (II), that is, C_{80} (6:D_{5h}) (see Figure 9 below). Such assignments are strongly supported by the good agreement between the experimental and the DFT-computed IR spectra (see Figure S1 in the Supporting Information).[12]

Figure 5 also clearly shows that the antisymmetric M–N stretching vibrational modes of $Gd_xSc_{3-x}N@C_{80}$ (I, II) (x = 0–3), which are correlated to the most intense low-energy IR lines in the region of 600–800 cm^{-1},[1,3–5,12] are sensitively dependent on the composition of the encaged $Gd_xSc_{3-x}N$ cluster. For $Gd_xSc_{3-x}N@C_{80}$ (I) (**1** and **2**), the antisymmetric M–N (M = Gd, Sc) stretching vibrational mode, which is twofold degenerate for a homogeneous cluster, was found to be split for the mixed $Gd_xSc_{3-x}N$ clusters.[12] Similarly, when the encaged Sc_3N cluster is replaced by the mixed $Gd_xSc_{3-x}N$ cluster within $Gd_xSc_{3-x}N@C_{80}$ (II) (**4** and **5**), such M–N stretching vibrational modes experience a similar splitting (see Table 1 and Figure S2 in the Supporting Information).

Figure 6 compares the experimental Raman spectra of $Gd_xSc_{3-x}N@C_{80}$ (I, II) (x = 0–3) obtained at 50 K.[15] Since the excitation energy of the laser wavelength of 647 nm

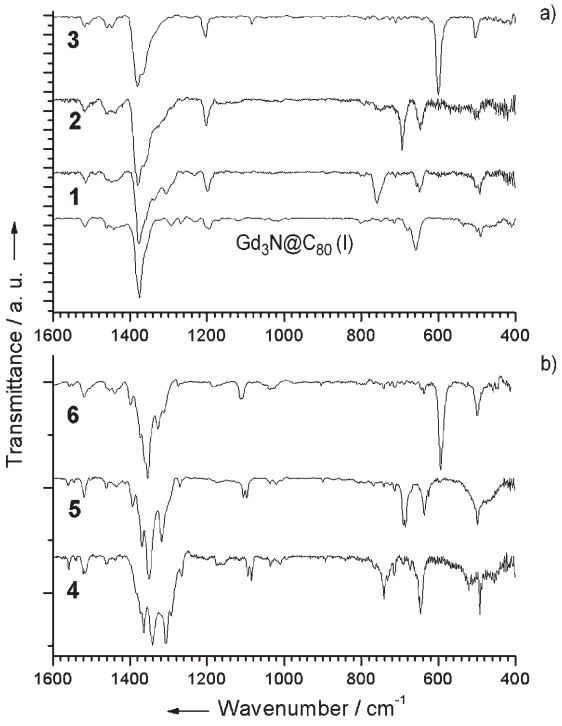

Figure 5. FTIR spectra of the two isomers of $Gd_xSc_{3-x}N@C_{80}$ (x = 0–3) (I, a; II, b). For clarity, the spectra of **1–3** and **5** and **6** are shifted upwards.

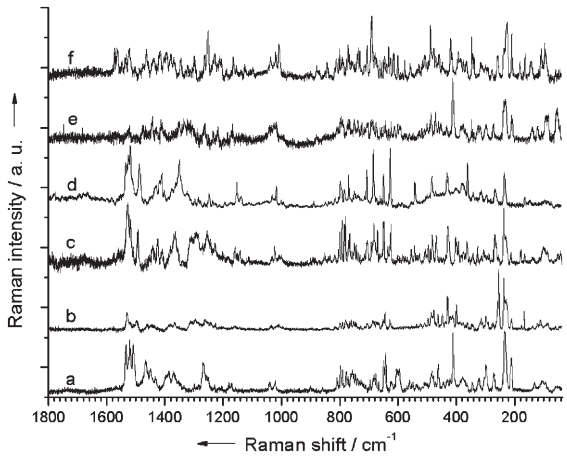

Figure 6. Raman spectra of **3** (a), **2** (b), **1** (c), $Gd_3N@C_{80}$ (d), **6** (e), and **5** (f). The spectra were obtained at 50 K and an excitation wavelength of 647 nm.

(1.92 eV) matches that of the lowest energetic electronic transitions of $Gd_xSc_{3-x}N@C_{80}$ (I, II) ($x=0$–3), strong resonance is observed for each fullerene and results in enhanced Raman intensity.[1,16] As reported before, the Raman spectrum of $Sc_3N@C_{80}$ (I) (**3**) consists of four regions: the tangential C_{80} modes between 1000 and 1600 cm^{-1}, a gaplike region of 815–1000 cm^{-1}, the radial breathing C_{80} cage modes in the range 200–815 cm^{-1} and the low-energy metal cage modes below 200 cm^{-1}.[16] Since the low-energy metal cage modes below 200 cm^{-1} provide essential information on the structure of the cluster and the cluster–cage interaction, a detailed analysis of this region is given below.

For $Gd_xSc_{3-x}N@C_{80}$ (I) ($x=0$–3) (Figure 6, curves a–d), despite the difference in the relative intensity of the Raman bands owing to the different resonance effects of the specific structures, both the tangential C_{80} modes and radial breathing C_{80} cage modes exhibit detectable shifts when x increases from 0 in $Sc_3N@C_{80}$ (I) to 3 in $Gd_3N@C_{80}$ (I). For instance, the most intense line in the region of the tangential C_{80} modes (1000–1600 cm^{-1}) is found at 1531, 1530, 1527, and 1520 cm^{-1} for $Sc_3N@C_{80}$ (I) (**3**), $GdSc_2N@C_{80}$ (I) (**2**), $Gd_2ScN@C_{80}$ (I) (**1**), and $Gd_3N@C_{80}$ (I), respectively. More dramatic differences in terms of the number of lines and shifts of the vibrational energies of lines are observed in the region of the radial breathing C_{80} cage modes (200–815 cm^{-1}), as clearly shown in Figure 6. These results indicate that the vibrational structure of $Gd_xSc_{3-x}N@C_{80}$ (I) (x=0–3) is dependent sensitively on the structure of the encaged $Gd_xSc_{3-x}N$ cluster. In terms of the overall Raman pattern, **1** is very close to $Gd_3N@C_{80}$ (I), while **2** exhibit closer resemblance to **3** ($Sc_3N@C_{80}$ (I), see also Figure S3 in the Supporting Information). In particular, the intensities of the tangential modes are comparable with those of the radial modes in the spectra of $Gd_3N@C_{80}$ (I) and **1**, while the further substitution of Gd by Sc atoms in **2** and **3** results in a dramatic decrease in relative intensities of the tangential modes. As the resonant Raman intensities are determined by the electronic excitations in the molecules under study, the changes in Raman intensity in the series of $Gd_xSc_{3-x}N@C_{80}$ (I) compounds point to the similarity of the electronic structures of $Gd_3N@C_{80}$ (I) and **1** on the one hand and of **2** and **3** on the other. This result is consistent with that obtained from the electronic absorption spectroscopic study described above. The similarity/difference in the electronic and vibrational structures of $Gd_xSc_{3-x}N@C_{80}$ (I) ($x=0$–3) is expected to result from the similarity/difference in the interaction between the cluster and the C_{80} cage, as discussed below.

A comparison of the Raman spectra of the isomer II of $Gd_xSc_{3-x}N@C_{80}$ ($x=0$, 1) (**5** and **6**) is also presented in Figure 6 (curves e, f).[15] With the decrease of the cage symmetry from I_h (isomer I) to D_{5h} (isomer II), the number of Raman lines increases in the region of both the tangential and radial modes of the C_{80} cage. The Raman spectrum of **5** [$GdSc_2N@C_{80}$ (II)] largely resembles that of **6** [$Sc_3N@C_{80}$ (II)], and this suggests similarity in the cluster–cage interactions in addition to the cage structures.

Cluster–cage interactions in $Gd_xSc_{3-x}N@C_{80}$ (I, II) ($x=1$, 2) studied by low-energy Raman spectroscopy: To probe the cluster–cage interaction in $M_3N@C_{80}$ nitride clusterfullerenes, the low-energy part of the vibrational pattern in the Raman spectrum was studied, because it is directly correlated to bond formation between the M_3N cluster and fullerene cage.[1,16] Figure 7 shows the low-energy part of the Raman

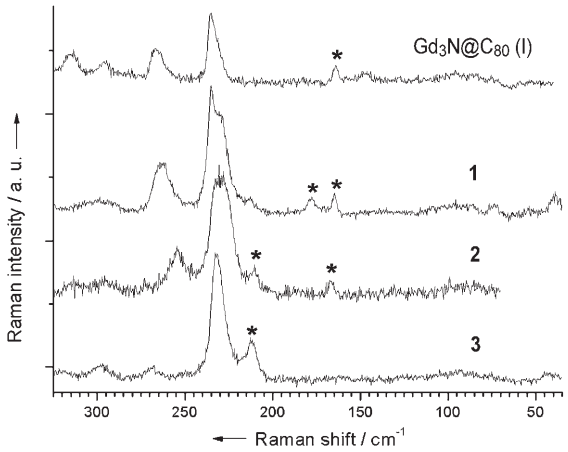

Figure 7. Low-energy Raman spectra of $Gd_xSc_{3-x}N@C_{80}$ (I) ($x=0$–3) obtained at 200 K. The asterisks mark the in-plane $Gd_xSc_{3-x}N$ cluster deformation modes (ν_{def}).

spectra of $Gd_xSc_{3-x}N@C_{80}$ (I) ($x=0$–3) clusterfullerenes obtained at 200 K, which in general consist of the radial C_{80} cage modes and of cluster-based modes ranging from 220 to 30 cm^{-1}.[1,16,17] While the radial C_{80} cage modes appear generally at frequencies down to 220 cm^{-1}, the cluster-based modes include the in-plane cluster deformation mode and the frustrated translations and rotations of the M_3N cluster, which provide crucial information on the interaction between the encaged nitride cluster and the C_{80} cage and consequently on the stability of the entire clusterfullerene.[1,4d,16]

As revealed in our previous study on the Raman spectra of a series of homogenous $M_3N@C_{80}$ (I) (M = Sc, Y, Gd–Tm) and DFT calculations, the medium-intensity Raman lines of $Sc_3N@C_{80}$ (I) at 210 cm^{-1} and $Gd_3N@C_{80}$ (I) at 165 cm^{-1} can be assigned to the frustrated in-plane cluster translation partially mixed with the in-plane M_3N deformation.[4d] Since this mode is directly related to cluster–cage bond formation, its frequency can serve as a measure of the strength of the cluster–cage interaction in the further analysis. As the cluster–cage force constant in $Sc_3N@C_{80}$ (I) was found to be smaller than that in $Gd_3N@C_{80}$ (I), it was concluded that the cluster–cage interactions in $Sc_3N@C_{80}$ (I) are significantly weaker than those in $Gd_3N@C_{80}$ (I).[4d] This mode, which is twofold degenerate for the homogeneous cluster, is expected to be split into two components for the $Gd_xSc_{3-x}N$ mixed cluster, as is the case for the antisymmetric metal–nitrogen stretching vibrational mode observed in the IR spectra. Indeed, in the Raman spectra of $Gd_xSc_{3-x}N@C_{80}$ (I) the two lines at 178/165 cm^{-1} for **1** ($x=$

2) and at 210/167 cm^{-1} for **2** ($x=1$) are assigned to these kind of vibrations. Recently, we have shown that the cluster–cage modes of all lanthanide-based $M_3N@C_{80}$(I) clusterfullerenes with homogeneous clusters can be adequately described by using the $Y_3N@C_{80}$ force field.[4d] Hence, to confirm the assignment of the cluster–cage modes in $Gd_xSc_{3-x}@C_{80}$(I), we computed their frequencies using the force field of the corresponding $Y_xSc_{3-x}@C_{80}$(I) molecules[12] and replacing the mass of Y by that of Gd. In good agreement with the experimental spectra, the calculations predict frequencies of 174/158 cm^{-1} in **1** and 205/160 cm^{-1} in **2**. Figure 8 shows the atomic displacement patterns for these

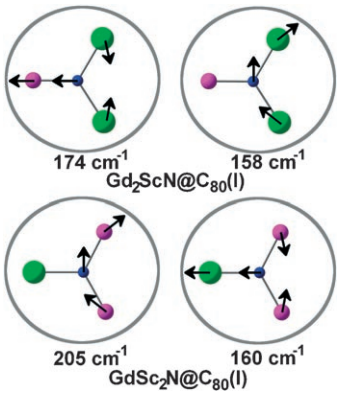

Figure 8. Schematic presentation of eigenvectors and frequencies of the mixed translation/deformation cluster modes (referred to as cluster-cage modes in the text) in **1** and **2**. The Sc, Gd, and N atoms are drawn in violet, green, and blue, respectively.

vibrations. As can be seen, the eigenvectors of the vibrations at 205 cm^{-1} in **2** and at 158 cm^{-1} in **1** are essentially the same as they would be in the homogeneous clusterfullerenes, and therefore their frequencies are close to those of the cluster–cage vibrations in $Sc_3N@C_{80}$ (I) and $Gd_3N@C_{80}$ (I), respectively. The second components are, however, more sensitive to the mixed nature of the cluster and occur at relatively low frequencies for both **1** and **2**.

To reveal the difference in cluster–cage interactions for the Sc- and Gd-bonding sites, we also computed the cluster–cage frequencies using the $Sc_3N@C_{80}$ (I) force field and replacing the mass of Sc atoms by that of Gd. The frequencies computed in this way for **1** and **2** are 162/143 cm^{-1} and 202/153 cm^{-1}, respectively. Clearly, the frequencies of vibrations which include displacements of Gd atoms are 10% smaller than those computed with the use of $Y_xSc_{3-x}N@C_{80}$ (I) ($x=1,2$) force fields and the experimental frequencies. This result confirms our earlier conclusion about the stronger cluster–cage interactions for the Y and lanthanide atoms than for Sc.[4d]

DFT calculations of the structures of $Gd_xSc_{3-x}N@C_{80}$ ($x=1$, 2): To establish the relation between cluster geometry and vibrational spectra of the mixed clusterfullerenes, we performed a series of DFT calculations for $Gd_xSc_{3-x}N@C_{80}$ (I, II) and $Y_xSc_{3-x}N@C_{80}$ (I).[12] The splitting of the metal–nitrogen stretching mode in $Gd_xSc_{3-x}N@C_{80}$ (I, II) is the anticipated consequence of the lowering of the effective symmetry of the $Gd_xSc_{3-x}N$ mixed cluster, which no longer has the threefold symmetry inherent to the homogeneous cluster. Recently, we developed a phenomenological model to describe the antisymmetric metal–nitrogen mode in the metal nitride clusters.[12] Using Y as a model for the lanthanide atoms, we computed the structures and vibrational spectra of a series of $Y_xSc_{3-x}N@C_{80}$ (I) clusterfullerenes at the PBE/TZ2P level.[12] The results indicate that in the $Y_xSc_{3-x}N@C_{80}$ (I) clusterfullerenes the nitrogen atom is displaced from the center of the molecule towards the Sc atoms, so that the Sc–N bond is considerably shorter than in $Sc_3N@C_{80}$ (I).[12] The same peculiarity of the cluster geometry was also revealed for $CeSc_2N@C_{80}$ (I) by X-ray crystallographic study.[9] As a result of these geometrical changes, the Sc–N stretching vibration experiences significant hardening on going from Sc_3N to M_2ScN (M = Gd, Er) (see Table 1 and Figure 9a–c). The same trend was also reported recently for a series of $Y_xSc_{3-x}N@C_{80}$ (I) ($x=0$–3)[10] and observed in this work for $Sc_3N@C_{80}$ (II), $Gd_2ScN@C_{80}$ (II), and $GdSc_2N@C_{80}$ (II).

In addition to hardening of the Sc–N mode, another concurrent effect of the aforementioned geometrical changes is that the M–N mode is softened in the series from M_3N to M_2ScN to MSc_2N clusters (M = Y, Gd, Er). Indeed, such a trend was observed for M = Er[3,12] (704/713→661→647 cm^{-1}) and recently for M = Y[10] (726/714→699→

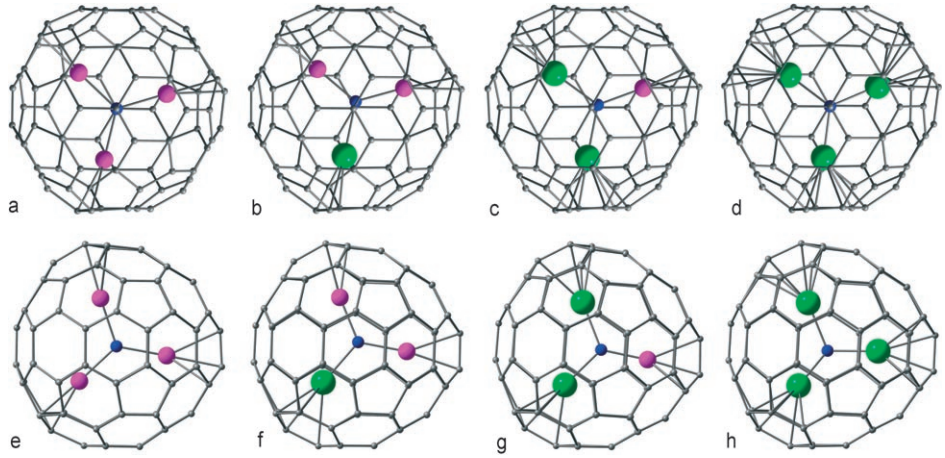

Figure 9. DFT-optimized structures of $Sc_3N@C_{80}$ (I_h, a), $GdSc_2N@C_{80}$ (I_h, b), $Gd_2ScN@C_{80}$ (I_h, c), $Gd_3N@C_{80}$ (I_h, d), $Sc_3N@C_{80}$ (D_{5h}, e), $GdSc_2N@C_{80}$ (D_{5h}, f), $Gd_2ScN@C_{80}$ (D_{5h}, g), and $Gd_3N@C_{80}$ (D_{5h}, h). The structures in a)–d) are viewed along the C_3 axis of the I_h-C_{80} cage, and for those in e–h the C_5 axis of D_{5h}-C_{80} cage lies in the plane of the paper. The Sc, Gd, and N atoms are drawn in violet, green, and blue, respectively.

647 cm^{-1}). However, the Gd–N mode does not show considerable softening (657→649→647 cm^{-1}, see Table 1 and Figure 9b–d), as expected on the basis of the calculations for $Y_xSc_{3-x}N@C_{80}$ (I). This result was explained by pyramidalization of the Gd_3N cluster in $Gd_3N@C_{80}$ (I).[12,18] Likewise, a pyramidal structure of the Gd_2ScN cluster was proposed within $Gd_2ScN@C_{80}$ (I), despite the fact that for the $Y_2ScN@C_{80}$ a planar structure of the cluster was predicted by DFT (see Table 2).[10,12] Apparently, the ionic radius of Y is smaller than that of Gd,[4d] and thus Y cannot be used as a full analogue of Gd when the structural peculiarities of the cluster are considered.

To study the structural peculiarities of the $Gd_xSc_{3-x}N$ clusters within $Gd_xSc_{3-x}N@C_{80}$, we performed scalar-relativistic calculations of the structures of $Gd_3N@C_{80}$, $Sc_3N@C_{80}$, and $Gd_xSc_{3-x}N@C_{80}$ clusterfullerenes. For the structures based on the C_{80} (I_h) cage, the cluster orientation with C_3 symmetry for the homogeneous clusters was used as found in our previous works (Figure 9a-d).[12] For the C_{80} (D_{5h}) cage our preliminary calculations showed coexistence of several almost isoenergetic minima, which considerably complicates the analysis. Hence, we chose the cluster orientation with respect to the carbon cage to be identical to that found by X-ray crystallography on $Tb_3N@C_{80}$ (II) (the structure of $Tb_3N@C_{80}$ (II) is disordered; the sites with the largest occupancies were used)[19] as starting point for geometry optimization of all clusters. For $Sc_3N@C_{80}$ (II), the calculations were also performed with coordinates revealed by X-ray crystallography on $Sc_3N@C_{80}$ (II).[20] The DFT-optimized structures are shown in Figure 9e–h, while their main structural features are summarized in Table 2 (note that the highest spin states were considered for $Gd_3N@C_{80}$ ($M=22$) and $Gd_2ScN@C_{80}$ ($M=15$), as only these states can be described by a single-determinant method such as DFT; see below).

In agreement with the X-ray data[18] and other DFT calculations,[21] the cluster in $Gd_3N@C_{80}$ (I) was found to be pyramidal with a pyramid height of $h=0.468$ Å. Pyramidal cluster configuration ($h=0.505$ Å) is also predicted for $Gd_3N@C_{80}$ (II), which has not yet been experimentally isolated (see Table 2). In the $Gd_xSc_{3-x}N@C_{80}$ clusterfullerenes, both the $GdSc_2N$ and Gd_2ScN clusters adopt planar structures in both I_h and D_{5h} cage isomers. Therefore, the previously suggested pyramidal structure of the cluster in $Gd_2ScN@C_{80}$ (I)[12] must be revised. In accordance with the IR spectra, the Sc–N bonds in the I_h cage are subject to considerable shortening in the sequence: Sc_3N→$GdSc_2N$→Gd_2ScN (2.026→1.964/1.968→1.910 Å, respectively). Thus, explaining the unprecedented increase in the Sc–N stretching frequency by 150 cm^{-1} on going from the Sc_3N to the Gd_2ScN cluster is straightforward. Similar but slightly longer Sc–N distances are also predicted for the clusters in the cage isomer II (Table 2), which is in line with the somewhat lower Sc–N stretching frequencies in **4** and **5** as compared to **1** and **2**, respectively (see Table 1).

To reveal the difference between the Gd- and Y-based mixed clusterfullerenes, we also optimized the geometric parameters for $Y_xSc_{3-x}N@C_{80}$ at the same level of theory. Though in general the systems show a substantial degree of similarity, the Sc–N bonds in $Y_xSc_{3-x}N@C_{80}$ are longer (1.974/1.979 Å for YSc_2N and 1.929 Å for Y_2ScN, as compared to those in $Gd_xSc_{3-x}N@C_{80}$ (1.964/1.968 Å for $GdSc_2N$ and 1.910 Å for Gd_2ScN), which is consistent with the lower Sc–N stretching frequency in YSc_2N (676 cm^{-1}) and Y_2ScN (736 cm^{-1}) compared to $GdSc_2N$ (694 cm^{-1}) and Gd_2ScN (759 cm^{-1}), respectively. Thus, a comparative analysis of DFT-predicted geometric parameters and the experimentally measured Sc–N stretching frequencies clearly demonstrates the high structural sensitivity of this mode, and hence semiquantitative estimations of the structural parameters of the cluster can based on the analysis of the vibrational spectra.

DFT calculations also support the dependence of the electronic structure of the mixed metallofullerenes on cluster composition, as discussed above on the basis of UV/Vis/NIR and Raman spectroscopic data. They predict that the HOMO–LUMO gaps for spin-up orbitals[22] listed in Table 2 show a gradual increase from $Sc_3N@C_{80}$ (I) (1.514 eV) to $Gd_3N@C_{80}$ (I) (1.624 eV) with the mixed clusters exhibiting intermediate values. An analogous trend is predicted for the clusterfullerenes based on the C_{80} (D_{5h}) cage (Table 2), albeit the HOMO–LUMO gaps for these molecules are systematically smaller than for the isomers based on $C_{80}(I_h)$. This is in reasonable agreement with the

Table 2. Selected DFT-predicted geometric parameters, HOMO–LUMO gaps (Gap), and exchange coupling constants J for $M_xSc_{3-x}N@C_{80}$ (M = Gd, Y).

	d(Sc–N) [Å]	d(M–N) [Å]	h[a] [Å]	Gap [eV]	J [cm^{-1}]
$Sc_3N@C_{80}$ (I) (**3**)	2.026		0.009	1.514	
$GdSc_2N@C_{80}$ (I) (**2**)	1.964, 1.968	2.168	0.009	1.559	
$Gd_2ScN@C_{80}$ (I) (**1**)	1.910	2.105, 2.110	0.019	1.588	−0.696
$Gd_3N@C_{80}$ (I)		2.080	0.468	1.624	−4.165[b]
$YSc_2N@C_{80}$ (I)	1.974, 1.979	2.147			
$Y_2ScN@C_{80}$ (I)	1.929	2.097, 2.100	0.012	1.573	
$Y_3N@C_{80}$ (I)		2.051	0.006	1.589	
$Sc_3N@C_{80}$ (II) (**6**)[c]	2.012, 2.029, 2.040		0.022	1.322	
$GdSc_2N@C_{80}$ (II) (**5**)	1.960, 1.982	2.173	0.043	1.344	
$Gd_2ScN@C_{80}$ (II) (**4**)	1.924	2.108, 2.108	0.003	1.383	−0.777
$Gd_3N@C_{80}$ (II)		2.085, 2.086, 2.094	0.505	1.413	−2.046

[a] Displacement of N atom out of the M_xSc_{3-x} plane predicted by DFT. [b] For $Gd_3N@C_{80}$ (I), almost the same J value was also computed with LSDA, mPBE, and OLYP functionals, that is, the form of exchange-correlation functional used is relatively unimportant for predicting the magnetic properties of these molecules. [c] The data listed for $Sc_3N@C_{80}$(II) (**6**) correspond to the structure shown in Figure 9e, in which the cluster has the same orientation with respect to the cage as in $Tb_3N@C_{80}$ (II).[19]. An alternative conformer obtained by optimization of the X-ray structure of $Sc_3N@C_{80}$ (II)[20] is 1.7 kJ mol^{-1} less stable and has a band gap of 1.350 eV.

experimental data. Note that Wang et al. recently reported similar changes in electronic properties for the $Y_xSc_{3-x}N@C_{80}$ (I) family,[10] and our DFT calculations also predict that the HOMO–LUMO gap increases in this system, up to 1.589 eV for $Y_3N@C_{80}$ (I).

Magnetic properties of $Gd_xSc_{3-x}N@C_{80}$ (x=1, 2) studied by DFT calculations: The large magnetic moment of the Gd atom localized on the 4f electrons implies that molecules with two or more Gd atoms can have different spin states. Within the limitation of a collinear alignment of the spin moments, only the highest spin state, that is, the state in which spin moments of all Gd atoms are parallel, can be described by a single determinant wave function and hence can be properly treated by DFT. At the same time, though low-spin states are not single-determinant in nature, magnetic properties of the system can still be predicted by DFT by using a broken-symmetry method proposed by Noodleman.[23a] For a two-nucleus system it was shown that though a determinant with antiparallel spins on two centers (so-called broken-symmetry state, denoted as $\uparrow\downarrow$ hereafter) is not an eigenfunction of the spin Hamiltonian, the energy difference between the high-spin state and a broken-symmetry state can be expressed in terms of the exchange parameter J of the Heisenberg spin Hamiltonian $H=-JS_1S_2$ by the simple relation $E(\uparrow\uparrow)-E(\uparrow\downarrow)=-2S^2J$ (S=7/2 for Gd). An analogous equation was also developed for a trinuclear system:[23c] $E(\uparrow\uparrow\uparrow)-E(\uparrow\downarrow\uparrow)=-2S^2J$, where $\uparrow\uparrow\uparrow$ describes the state with parallel spin alignment (M=22), while $\uparrow\downarrow\uparrow$ is a broken-symmetry state with two parallel and one antiparallel spins (M=8). Therefore, to reveal the magnetic coupling of Gd atoms in $Gd_3N@C_{80}$ and $Gd_2ScN@C_{80}$, we optimized the geometry for broken-symmetry states and estimated exchange parameter J (Table 2) from the energy difference to the highest spin states (M=22 and 15, respectively). Both for $Gd_3N@C_{80}$ and $Gd_2ScN@C_{80}$, weakly antiferromagnetic coupling is predicted by theory, with $-J$ values of 2–4 cm^{-1} for $Gd_3N@C_{80}$ (I, II) and 0.7–0.8 cm^{-1} for $Gd_2ScN@C_{80}$ (I, II). Our data agree with the recent DFT study of Lu et al.,[21a] who also predicted an antiferromagnetic ground state for $Gd_3N@C_{80}$ (I) using either PBE or PBE+U methods and a numerical DNP basis set. At the same time, Qian et al.[21b] found a ferromagnetic ground state for $Gd_3N@C_{80}$ (I) using the LDA+U approach and a plane-wave basis set augmented with pseudopotentials. For $Gd_2ScN@C_{80}$, the magnitude of the J values is comparable to but somewhat higher than the values for a series of dinuclear Gd complexes studied by Roy et al.[23b] Further experimental and theoretical studies to clarify the magnetic properties of $Gd_xSc_{3-x}N@C_{80}$ are underway.

Conclusion

In summary, we have reported the first synthesis of the two isomers of Gd/Sc mixed-metal nitride clusterfullerenes $Gd_xSc_{3-x}N@C_{80}$ (**1**, **2**, **4**, **5**) and their facile isolation by recycling HPLC. Based on the HPLC profile, the yield of $Gd_xSc_{3-x}N@C_{80}$ (I, II) (x=1, 2) relative to the homogenous clusterfullerenes $Sc_3N@C_{80}$ [I (**3**), II (**6**)] was calculated to be 0.56:2.2:1 for **1**:**2**:**3** and 0.36:0.8:1 for **4**:**5**:**6**, that is, the yield of **2** is enhanced in comparison with that of **3**, whereas the yield of $Gd_xSc_{3-x}N@C_{80}$ (II) (**4** and **5**) is decreased as compared to **6**. While **1**, **2, 4, 5** are all stable fullerenes with large optical band gaps, a UV/Vis/NIR spectroscopic study revealed that **1** has greater similarity to $Gd_3N@C_{80}$ (I), while **2** seems to more closely resemble $Sc_3N@C_{80}$ (I). The quite similar overall absorption features of **4** and **5** suggest close resemblance of the their electronic structures. According to vibrational (FTIR and Raman) spectroscopic studies and DFT calculations, the cage structures of $Gd_xSc_{3-x}N@C_{80}$ (I) (**1** and **2**) are assigned to the I_h isomer, while $Gd_xSc_{3-x}N@C_{80}$ (II) (**4** and **5**) are shown to have a D_{5h} cage. The cluster–cage ($Gd_xSc_{3-x}N$–C_{80}) interactions in $Gd_xSc_{3-x}N@C_{80}$ (I) (**1**, **2**) were studied by low-energy Raman spectroscopy, which led to the assignment of the cluster–cage modes. The splitting of the metal–nitrogen stretching vibrational mode in $Gd_xSc_{3-x}N@C_{80}$ (I, II) was studied in detail and rationalized by the geometry parameters of the cluster predicted by DFT calculations. Finally, scalar-relativistic DFT calculations were performed to study the magnetic properties of the $Gd_xSc_{3-x}N@C_{80}$ (I, II) molecules. Detailed magnetic measurements on these and other mixed-metal clusterfullerenes are underway.

Experimental Section

$Gd_xSc_{3-x}N@C_{80}$ (I, II) (x=1, 2) were produced by a modified Krätschmer–Huffman DC arc-discharge method with the addition of NH_3 (20 mbar), as described elsewhere.[1,3–5,12] Briefly, a mixture of Gd_2O_3 and Sc_2O_3 (99.9%, MaTeck GmbH, Germany) and graphite powder was used (molar ratio of Gd:Sc:C=1:1:15). After DC arc discharge, the soot was pre-extracted by acetone and further Soxhlet-extracted by CS_2 for 20 h. Fullerenes were isolated by two-step HPLC. In the first step running in a Hewlett-Packard instrument (series 1050), a linear combination of two analytical 4.6×250 mm Buckyprep columns (Nacalai Tesque, Japan) was applied with toluene as eluent. The second-stage isolation was performed by recycling HPLC (Sunchrom, Germany) on a semipreparative Buckyprep-M column (Nacalai Tesque, Japan) with toluene as eluent. A UV detector set to 320 nm was used for fullerene detection in both stages. The purity of the isolated products was checked by LD-TOF MS analysis running in both positive- and negative-ion modes (Biflex III, Bruker, Germany).

Sample preparation and experimental details for UV/Vis/NIR and FTIR spectroscopic measurements were described previously.[3–5] For Raman measurements, 100–200 μg of $Gd_xSc_{3-x}N@C_{80}$ (I, II) (x=1, 2) was drop-coated onto single-crystal KBr disks. The residual toluene was removed by heating the polycrystalline films in a vacuum of 2×10^{-6} mbar at 235°C for 3 h. Raman scattering was excited by the 647 nm emission lines of an Kr^+ ion laser (Innova 300 series, Coherent, USA). The scattered light was collected in a 180° backscattering geometry and was analyzed by a T 64000 triple spectrometer (Jobin-Yvon, France) whose spectral band pass was set to 2 cm^{-1}.

Scalar-relativistic[24] DFT computations were performed with the PRIRODA package[25] and PBE density functional.[26] A full-electron DZP-quality basis set (A1 in ref. [25c]) implemented in the code was used for all atoms.

Acknowledgement

We cordially thank Ms. K. Leger, Mr. F. Ziegs, and Mrs. H. Zöller for technical assistance. S.Y. and M.K. thank the Alexander von Humboldt (AvH) Foundation for financial support. Computer time at the Research Computing Center of the Moscow State University for A.P. is gratefully acknowledged.

[1] For recent reviews, see: a) L. Dunsch, S. Yang, *Small*, **2007**, *3*, 1298–1320; b) L. Dunsch, S. Yang, *Phys. Chem. Chem. Phys.* **2007**, *9*, 3067–3081; c) L. Dunsch, S. Yang, *Electrochem. Soc. Interface* **2006**, *15(2)*, 34–39.

[2] S. Stevenson, G. Rice, T. Glass, K. Harich, F. Cromer, M. R. Jordan, J. Craft, E. Hajdu, R. Bible, M. M. Olmstead, K. Maitra, A. J. Fisher, A. L. Balch, H. C. Dorn, *Nature* **1999**, *401*, 55–57.

[3] L. Dunsch, M. Krause, J. Noack, P. Georgi, *J. Phys. Chem. Solids* **2004**, *65*, 309–315.

[4] a) S. F. Yang, L. Dunsch, *J. Phys. Chem. B* **2005**, *109*, 12320–12328; b) S. F. Yang, L. Dunsch, *Chem. Eur. J.* **2006**, *12*, 413–419; c) S. F. Yang, M. Kalbac, A. Popov, L. Dunsch, *Chem. Eur. J.* **2006**, *12*, 7856–7862; d) S. F. Yang, S. Troyanov, A. Popov, M. Krause, L. Dunsch, *J. Am. Chem. Soc.* **2006**, *128*, 16733–16739; e) S. F. Yang, A. Popov, L. Dunsch, *Angew. Chem.* **2007**, *119*, 1278–1281; *Angew. Chem. Int. Ed.* **2007**, *46*, 1256–1259; f) A. A. Popov, L. Dunsch, *J. Am. Chem. Soc.* **2007**, *129*, 11835–11849.

[5] a) M. Krause, L. Dunsch, *ChemPhysChem* **2004**, *5*, 1445–1449; b) M. Krause, J. Wong, L. Dunsch, *Chem. Eur. J.* **2005**, *11*, 706–711; c) M. Krause, L. Dunsch, *Angew. Chem.* **2005**, *117*, 1581–1584; *Angew. Chem. Int. Ed.* **2005**, *44*, 1557–1560; d) M. Krause, A. Popov, L. Dunsch, *ChemPhysChem* **2006**, *7*, 1734–1740.

[6] a) M. M. Olmstead, A. de Bettencourt-Dias, J. C. Duchamp, S. Stevenson, H. C. Dorn, A. L. Balch, *J. Am. Chem. Soc.* **2000**, *122*, 12220–12226; b) R. M. Macfarlane, D. S. Bethune, S. Stevenson, H. C. Dorn, *Chem. Phys. Lett.* **2001**, *343*, 229–234; c) I. N. Ioffe, A. S. Ievlev, O. V. Boltalina, L. N. Sidorov, H. C. Dorn, S. Stevenson, G. Rice, *Int. J. Mass Spectrom.* **2002**, *213*, 183–189.

[7] S. Stevenson, P. W. Fowler, T. Heine, J. C. Duchamp, G. Rice, T. Glass, K. Harich, E. Hajdu, R. Bible, H. C. Dorn, *Nature* **2000**, *408*, 427–428.

[8] E. B. Iezzi, J. C. Duchamp, K. R. Fletcher, T. E. Glass, H. C. Dorn, *Nano Lett.* **2002**, *2*, 1187–1190.

[9] X. L. Wang, T. M. Zuo, M. M. Olmstead, J. C. Duchamp, T. E. Glass, F. Cromer, A. L. Balch, H. C. Dorn, *J. Am. Chem. Soc.* **2006**, *128*, 8884–8889.

[10] N. Chen, L. Z. Fan, K. Tan, Y.Q Wu, C. Y. Shu, X. Lu, C. R. Wang, *J. Phys. Chem. C* **2007**, *111*, 11823–11828.

[11] P. W. Fowler, D. E. Manolopoulos, *An Atlas of Fullerenes*, Clarendon Press, Oxford, **1995**.

[12] S. F. Yang, M. Kalbac, A. Popov, L. Dunsch, *ChemPhysChem* **2006**, *7*, 1990–1995.

[13] N. Chen, E. Zhang, K. Tan, C. R. Wang, X. Lu, *Org. Lett.* **2007**, *9*, 2011–2013.

[14] $Gd_3N@C_{80}$ (II) was reported in ref. [5c] but has not been isolated yet.

[15] The amount of $Gd_2ScN@C_{80}$ (II) isolated so far was not sufficient for Raman spectroscopic study.

[16] M. Krause, H. Kuzmany, P. Georgi, L. Dunsch, K. Vietze, G. Seifert, *J. Chem. Phys.* **2001**, *115*, 6596–6605.

[17] Note that a more complex spectroscopic pattern is observed at lower temperatures with the number of low-energy Raman lines exceeding that expected for these molecules on the base of the calculations (see Figure S3 in the Supporting Information). The additional lines could be caused by crystal-field splitting (see ref. [16]) as well as by different cluster positions inside the cage. Their detailed assignment is not possible at this time.

[18] S. Stevensen, J. P. Phillips, J. E. Reid, M. M. Olmstead, S. P. Rath, A. L. Balch, *Chem. Commun.* **2004**, 2814–2815.

[19] T. M. Zuo, C. M. Beavers, J. C. Duchamp, A. Campbell, H. C. Dorn, M. M. Olmstead, A. L. Balch, *J. Am. Chem. Soc.* **2007**, *129*, 2035–2043.

[20] T. Cai, L. S. Xu, M. R. Anderson, Z. X. Ge, T. M. Zuo, X. L. Wang, M. M. Olmstead, A. L. Balch, H. W. Gibson, H. C. Dorn, *J. Am. Chem. Soc.* **2006**, *128*, 8581–8589.

[21] a) J. Lu, R. F. Sabirianov, W. N. Mei, .Y. Gao, C. Duan, X. Zeng, *J. Phys. Chem. B* **2006**, *110*, 23637–23640; b) M. C. Qian, S. V. Ong, S. N. Kahnna, M. B. Knickelbein, *Phys. Rev. B* **2007**, *75*, 104424.

[22] a) S. Abdelouahed, B. Baadji, M. Alouani, *Phys. Rev. B* **2007**, *75*, 094428, and references therein b) The gaps for the spin-up and spin-down orbitals are considerably different. This can be explained by the importance of the correlation effects for the highly localized 4f orbitals. It was shown for Gd that conventional DFT methods significantly underestimate the splitting between occupied and unoccupied 4f bands and the energies of unoccupied 4f-based states.[22a] At the same time, the energies of 5d and 6s bands are predicted with reasonable accuracy.[22a] Hence, we consider that the gaps for spin-down orbitals predicted in this work for $Gd_xSc_{3-x}N@C_{80}$ are affected by the inadequate treatment of the vacant 4f orbitals of Gd, and hence physically meaningful values can be obtained only for spin-up orbitals, which are therefore discussed here. Note that the description of the 4f states can be improved by introduction of the Hubbard U Hamiltonian via the DFT+U method,[22a] and such an option for $Gd_xSc_{3-x}N@C_{80}$ will be addressed in future work.

[23] a) L. Noodleman, *J. Chem. Phys.* **1981**, *74*, 5737–5743; b) L. E. Roy, T. Hughbanks. *J. Am. Chem. Soc.* **2005**, *128*, 568–575; c) L. Noodleman, D. A. Case, A. Aizman, *J. Am. Chem. Soc.* **1988**, *110*, 1001–1005.

[24] a) K. G. Dyall, *J. Chem. Phys.* **1994**, *100*, 2118–2127; b) D. N. Laikov, Abstracts DFT2000 Satellite Symposium of the 10th Int. Congress of Quantum Chemistry, France, June 2000, P43.

[25] a) D. N. Laikov, *Chem. Phys. Lett.* **1997**, *281*, 151–156; b) D. N. Laikov, Yu. A. Ustynyuk, *Russ. Chem. Bull. Int. Ed.* **2005**, *54*, 820–826; c) D. N. Laikov, *Chem. Phys. Lett.* **2005**, *416*, 116–120.

[26] J. P. Perdew, K. Burke, M. Ernzerhof, *Phys. Rev. Lett.* **1996**, *77*, 3865.

Received: October 9, 2007
Published online: January 9, 2008

